Combustion and Flame 207 (2019) 327–341

Contents lists available at ScienceDirect

Combustion and Flame

journal homepage: www.elsevier.com/locate/combustflame

Combustion details of raw and torrefied biomass fuel particles with individually-observed size, shape and mass

Aidin Panahi[a], Nikita Vorobiev[b], Martin Schiemann[b], Mahmut Tarakcioglu[a], Michael Delichatsios[a], Yiannis A. Levendis[a,*]

[a] Mechanical and Industrial Engineering Department, Northeastern University, Boston, MA, USA
[b] Ruhr University Bochum, Bochum, Germany

ARTICLE INFO

Article history:
Received 7 February 2019
Revised 11 June 2019
Accepted 12 June 2019
Available online 25 June 2019

Keywords:
Single particle
Biomass
Combustion
Cinematography
Pyrometry
Burning rates

ABSTRACT

A unique approach and proposed methodology was implemented to determine char burning rates in conjunction to their prevailing structure from detailed results on the combustion histories of small biomass fuel particles, exposed to elevated temperatures (>1000 K) at very high heating rates (10^4–10^5 K/s). Analogous conditions typically prevail in pulverized fuel utility boilers for power generation. Individual particles of pre-measured size, shape, aspect ratio and mass from five different types of raw and torrefied biomass were selected for this study. The particles were injected into a transparent drop-tube furnace, electrically heated to 1400 K, where they were rapidly heated, ignited and burned in air. Temperature-time histories of the individual particles were recorded pyrometrically and were used to assess their individual combustion rates. These particles burned in distinct volatile and char phases. A published phenomenological combustion model for carbonaceous fuel particles was enhanced and applied to the experimental data to calculate the char burning rates. Important information on the nature of these chars, which formed inside volatile matter envelope flames, was obtained by juxtaposition of the knowledge of their original properties with the pyrometric observations and the numerical simulations. It was concluded that, under the conditions of these experiments, chars of most types of biomass consisted of thin-wall cenospherical particles. The modeling results show that this predominant particle structure needs to be considered for reliable burnout predictions.

1. Introduction

Global primary energy consumption is expected to grow at an annual rate of 1.6% by 2050 [1–3]. Energy harvesting from combustion of fossil fuels is still dominant, however it generates pollution and greenhouse gases, such as carbon dioxide. Combustion of coal in particular, currently accounts for 45% of the carbon dioxide emissions [4,5]. Recently, 37% of the total power generation in the world was from coal-burning power plants [6–8]. A number of techniques and methods have been proposed for reducing emissions of greenhouse gases from coal combustion [9–13]. Among the less-expensive alternatives, co-firing with renewable biomass is gaining popularity with the power generation utilities [14]. Since growth of biomass utilizes atmospheric CO_2, co-firing coal with renewable biomass can reduce the net CO_2 emissions [15–22]. Biomass has some disadvantages compared to coal (low calorific value, high moisture content, low grindability, high biodegradability, fine particulate emissions [23–25], mainly those of submicron particles, and some types of biomass have notoriously high emissions of chlorine and alkalis [21,26] which may require changes in flue-gas treatment. Torrefaction, a mild pyrolysis, can be used to improve on most of such shortcomings of raw biomass as a fuel [24,27–32]. Hence, torrefied biomass can be a more suitable (than raw biomass) alternative fuel to be fired or co-fired with coal in existing large-scale pulverized coal boilers [33–38]. The literature on burning pulverized coal as a fuel is voluminous and the ignition mode, combustion behavior and reaction rates of coal particles have been extensively documented in a number of studies using thermogravimetry, cinematography, pyrometry and other techniques [39–52]. In the case of lignocellulosic biomass, there have been a plethora of studies related to fire science, which were conducted at low heating rates to moderate temperatures, recently reviewed in by Richter and Reim [53] to model burning rates of timber. In those, mostly thermogravimetric (TGA) experiments,

* Corresponding author.
E-mail address: y.levendis@neu.edu (Y.A. Levendis).

https://doi.org/10.1016/j.combustflame.2019.06.009
0010-2180/

Nomenclature

Latin letters

A	outer surface area [m^2]
a_0	ash content of the original biomass sample
a_{char}	ash content of the char
c_p	heat capacity [J/(kg K)]
c	concentration [mol/m^3]
D	diffusion coefficient [m^2/s]
d	diameter [m]
F^*	shape coefficient
Δh	molar heat of reaction [J/mol]
j_C^p	specific reaction rate [mol C/(m^2 s)]
k	calibration constant [1/K]
l^*	characteristic length [m]
m	mass [kg]
$\dot{n}_c^p$	carbon conversion rate [mol/s]
p	partial pressure [Pa]
P	total pressure [Pa]
s	cenosphere shell thickness
R	ideal gas constant [J/(K mol)]
T	temperature [K]
t	time
v	velocity [m/s]
V	volume [m^3]
VM	volatile matter

Greek Letters

γ	volume change in boundary layer
ε	emissivity
η	normal direction
κ	Péclet number
λ	thermal conductivity [W/(m K)]
ν	stoichiometric coefficient
ρ	density [kg/m^3]
ρ_{app}	char apparent density [kg/m^3]
ρ_{bulk}	bulk biochar density [kg/m^3]
σ	Stefan–Boltzmann constant [W/(m^2 K^4)]
ψ	fraction of carbon that becomes CO_2
φ	porosity

Indices

c	carbon
ext	external surface
g	gas
i	any species
O_2	oxygen
p	particle
w	wall

timber experienced low heating rates in the order of 1 to 60 K/min (0.02–1 K/s). In recent years, there has also been a significant number of publications on fast pyrolysis and combustion of biomass particles under high heating rates (10^4 K/s) targeting applications of energy harvesting in suspension boilers. Such works include the investigations of Refs. [54–73]. There is also a limited number of reports on the combustion behavior of torrefied biomass as a fuel at high heating rates including [22,37,74–79]. Such biomass pyrolysis and combustion studies by the authors and others have shown that the structural transformations of biomass are exceedingly different at very high heating rates, as compared to those at moderate or low heating rates. Hence, while the low heating rate studies provide valuable information on many aspects of the pyrolysis and combustion of cellulosic biomass for construction applications, they do not simulate the combustion of pulverized biomass, as a fuel, under suspension boiler conditions where very high heating rates (10^4–10^5 K/s) and high temperatures (well above 1000 K) prevail. Under such conditions fuel particles undergo flash pyrolysis, the release of volatiles is nearly explosive, and the residual particles undergo fusion and concomitant spherodization and pore formation [54,57]. In fact, the speed of pyrolysis has been found to affect the reactivity of the generated chars [54].

There have been modeling efforts for pyrolysis (charring) of biomass, see for instance [53,80,81] and of pyrolysis and combustion of biomass [82]. Biomass particle combustion studies draw from similarities with coal combustion, which has been studied extensively. However, most of the studies in the literature on the combustion of pulverized coal particles dealt with particles that typically do not vary widely in size or shape, as coal is friable, grinds easily and can be sieved to particles of separable size cuts. To the contrary, biomass does not grind easily due to its fibrous and tenacious nature [83] and structure [84]. Hence, pulverized biomass particles vary widely in size and shape and they have much higher aspect ratios than coal. Previous investigations (e.g. Panahi et al. [37], Magalhães et al. [72], Momeni et al. [85], Mason et al. [70] and Mock et al. [69]) assessed the combustion characteristics of biomass by averaging the behavior of many particles in a size cut. However, such highly differentiated particles, often of very high aspect ratios (e.g. needles), even if classified to be in the same size cut, they can burn at exceedingly disparate rates and temperatures. This fact makes the simulation of their combustion behaviors by existing kinetic models of pulverized solid fuels challenging and problematic. Therefore, the goal of this research is to generate detailed data on the combustion behaviors of individually-observed biomass fuel particles of various kinds/origins, both raw and torrefied. Such details pertain to the physical transformations that occur during their heat up at very high rates, devolatilization and combustion. The acquired knowledge can facilitate the calculation of more accurate combustion rates, improve the kinetic modeling efforts on biomass combustion, and support the understanding of processes which need to be considered during biomass combustion. Particles of small size, expediently heated to high temperatures are of particular interest in this study, as such conditions approximate pulverized fuel (p.f.) combustion in suspension boilers. Entire temperature-time histories of burning individually-assessed biomass particles, of a-priori known mass, size and shape were obtained with concurrently-applied pyrometric and cinematographic techniques and are presented herein for the first time. A previously published kinetic model for char oxidation at relevant conditions by Vorobiev et al. [79] and Schiemann et al. [86] was adapted to fit the char portion of experimentally-recorded temperature profiles of pre-weighted individual raw and torrefied biomass particles and then calculate their time-resolved carbon conversion progress. Model upgrades were needed to deal with the particular structural aspects of these “cenospheric” chars. Note that this model was validated first with the combustion temperature-time histories of the well-characterized and known-size synthetic cenospheres of Levendis and Flagan [87], before it was applied to the individual biomass char particles of unknown size and structure. Burning of any of these chars takes place in a combustion regime which includes chemistry and boundary/pore diffusion. The current study does not focus on chemical effects, which have been reported in the literature, but focuses on experimental data on single particles to elucidate structural changes that affect char combustion. The predominant hypothesis in this work has been that biomass particles, both raw and torrefied, upon experiencing flash pyrolysis undergo softening and fusion and form light cenospheric chars with large voids and membrane-like porous walls. Their high temperature combustion then takes place at the upper end of Regime II or in Regime III [54,88].

2. Materials and methods

2.1. Preparation of samples

In preparation for this study, samples of different types of biomass fuels were selected based on those typically used in large-scale power generation boilers. Corn straw was harvested in the Harbin province of China and was provided by Harbin Institute of Technology. Miscanthus originated from an agricultural farm in Germany (Sieverdingbeck-Agrar), and it was provided by Ruhr-University Bochum, Germany. Eucalyptus and pine originated from UK forestry; willow was harvested from UK Agronomy Research Corp; these three samples were provided by the University of Leeds, UK, in the form of chips. The biomass samples were not subjected to any pre-processing.

Torrefaction of all raw biomass samples was carried out in laboratory-scale horizontal muffle furnaces in nitrogen. The furnaces were charged with 10–15 millimeter-size particles of biomass in a wide porcelain boat to ensure sufficient space between particles and, subsequently, they were heated to 275 °C, with heating rates in the order of 10 °C/min. Upon reaching the final temperature, each sample was heat-treated at constant conditions for 30 min. In recent works in this laboratory, it has been observed that the torrefaction process reduces the particle aspect ratios [89,90]. The chemical compositions of the raw and torrefied biomass fuels are shown in Table 1. Proximate and Ultimate analysis were carried out on fine (50 µm) particles according to standard protocols EN 14774-3, EN15148, EN 14775 and EN 15104 as described in [71,91]. Proximate analysis was performed using a Thermogravimetric Analyzer (*TA Instruments Q5000*). Carbon, hydrogen, nitrogen and sulfur mass fractions in the fuels were measured using a *Flash EA1112* elemental analyzer. Oxygen was measured using a *Thermo EA2000* elemental analyzer. These measurements were conducted at the University of Leeds and the uncertainty in the values, listed in Table 1, was reported to vary between 0.05% to 0.6%. Proximate analysis shows torrefied biomass had volatile mass fractions that were lower by 2–11 wt% than those of raw biomass, except eucalyptus and pine. Eucalyptus and pine have large amounts of aromatic oils and tars and torrefaction has broken these materials into smaller molecular weight compounds; hence, the volatile matter of torrefied eucalyptus and pine has been increased [92]. Finally, the mass fraction of ash increased in general, with the exception of corn straw.

2.2. Experimental apparatus and approach

The combustion studies of free-falling individual biomass particles were carried out in an electrically heated, laminar-flow, vertical drop-tube furnace (DTF), manufactured by *ATS*, at a constant wall temperature of T_{wall}=1400 K. The resulting axial gas temperature profile has been measured to be approximately constant at T_{gas} = 1350 K [93,94]. The radiation cavity of the furnace is 25 cm long and is heated by hanging molybdenum disilicide elements. A sealed 7 cm i.d. transparent quartz tube was fitted in this furnace. Air was introduced into the radiation cavity of the furnace through a water-cooled stainless steel injector at a flow-rate of 0.5 L/min, measured at 25 °C, 1 bar. The selected biomass particles, both raw and torrefied, were subsequently weighted in a microbalance (Sartorius ME36S) with accuracy of ±10 µg and they were also photographed under an optical microscope (Fisher Scientific). Thereafter, the particles were individually introduced through a small hole at the top of the injector by the use of tweezers. Entering the radiation cavity (drop tube) of the furnace they experienced high heating rates (10^4 K s^{-1}). Optical access to the radiation zone of the furnace was achieved through three observation ports: one at the top and two diagonally situated at the sides of the furnace, as shown in Fig. 1. The volatile envelope flame and char temperatures of the burning particles were pyrometrically measured from the top of the furnace, along the vertical axis of the furnace. Details of the pyrometer optics, electronics, calibration, and performance are given by Levendis et al. [95]. Pyrometric measurement uncertainties stem from particle to particle variations in size, shape and structure, and from uncertainties in the pyrometric method. Uncertainties from particle to particle variations, can be in the order of 100 K [79], as shown in an ensuing section of this work. Pyrometric method uncertainties can be commensurate, as discussed in Refs. [39,95]. Such uncertainties are associated with the flame and char emissivities, which in both cases were assumed (based on Ref. [95]) to be independent of wavelength, in the range of wavelengths used in this pyrometer. Uncertainties also arise from the instrument calibration, which in this case was based on a pre-calibrated lamp supplied by the US. National Institute of Standards and Technology (NIST), as well as from the transmissivities of the pyrometric interference and dichroic filters, and from the responsivities of the photodetectors. In prior work on coal particle combustion in this laboratory it was shown that the uncertainty of the temperature flame measurement in air combustion was approx. 60 K, depending on the soot spectral emissivity model used (one of which was the gray assumption), see Fig. 7 of Ref. [96]. The char temperature can also be affected by the uncertainty of the char spectral emissivity, which was shown to be approx. 40 K [97]. Overall, it may be reasonable to assume an uncertainty of 100 K in the measured particle temperature profiles of Figs. 2 and 3 herein. Perhaps the uncertainty is less than this value, since the temperature of a type S platinum/rhodium thermocouple, heated by a Bunsen burner flame, was pyrometrically measured with an uncertainty of

Table 1
Chemical compositions of raw and torrefied biomass.

Rank/fuel		Herbaceous biomass				Woody biomass					
		Corn Straw		Miscanthus		Eucalyptus		Willow		Pine	
Content	Basis	R	T	R	T	R	T	R	T	R	T
Proximate analysis											
Moisture, wt%	as received	2.6	1.2	3.5	0.6	6	1.5	4.1	0.9	4.5	0.9
Ash, wt%	dry	9.4	8.9	3	3.4	0.8	1.6	1.8	3.1	1.9	3.7
Volatile matter, wt%	as received	77.2	66.6	83.9	79.6	77.6	78.8	78.7	77.1	77.3	81.9
Fixed carbon, wt%	as received	10.9	23.3	9.7	16.4	15.5	18.2	15.4	18.9	16.3	13.6
Ultimate analysis											
Carbon, wt%	dry	42.3	51.5	47.5	51.2	48.7	52.1	49.4	52.2	46.5	49.7
Hydrogen, wt%	dry	5.6	5.3	6	5.7	6.3	5.6	6.4	5.5	5.2	5.5
Oxygen, wt%	dry	41.5	33.3	43.1	39.7	44.1	40.4	41.5	38.8	45.1	41
Nitrogen, wt%	dry	1.2	1.1	0.2	0.1	0.1	0.3	0.4	0.5	1.3	0.2
Sulphur, wt%	dry	<0.1	<0.1	0.2	<0.1	<0.1	<0.1	<0.1	<0.1	<0.1	<0.1

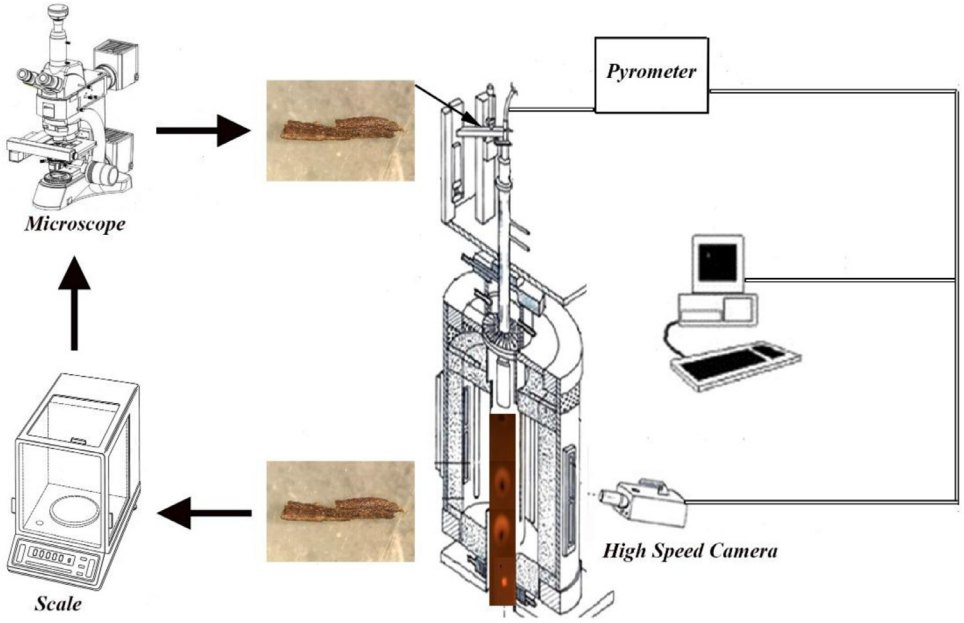

Fig. 1. Schematic of the experimental setup used in this work (not to scale), including a microbalance, an optical microscope, a drop-tube furnace, an optical pyrometer and a high-speed camera.

only 20–30 K; the pyrometric temperature was 1760 ± 20 when the thermocouple recorded 1730 ± 5 K. The former value was obtained using published thermocouple type-S spectral emissivities for the 650 and 810 µm channels from Ref. [98] and, since the emissivity of type-S thermocouple was not available, the emissivity of platinum was used for the 998 µm channel from Ref. [99]. The voltage signals generated by the photo-detectors of the pyrometer were amplified and recorded by a microcomputer using *LabView* software. Temperature was deduced from the pyrometric voltage signals as outlined in previous work [39]. High-speed cinematography was used to record the combustion histories of the individual particles through one of the two quartz windows on the sides of this furnace. An *Edgertronic* self-contained digital high-speed high-resolution broadband video camera was used at a speed of 1000 frames per second. The camera was fitted with a *Nikon* 50 mm F1.8 D-lens.

3. Experimental results and discussion

3.1. Concurrent cinematography and pyrometry of individual particles

For each biomass type, ten individual particles were first weighted and then photographed under an optical microscope. Photographs, mass and two initial dimensions of each individual particle are shown in Table A1 in the Supplementary Material A. The combustion of each one of these small particles with individually-known shape size and mass was observed with concurrent high-speed cinematography and pyrometry, to document their entire time-resolved profiles. Synchronizing all diagnostic methods for the first time to obtain concurrent observation proved to be a challenging task and often cinematography was not complete, as many particles moved out of the field of observation. The three most successfully monitored burning particles from each type of biomass are displayed in Figs. 2 and 3, for raw and torrefied biomass respectively. Most of the biomass particles were in the shape of needles and, thus, their widths and depths were nearly the same, whereas their lengths were much longer. However, the three dimensions of those biomass particles that were in the shape of flakes, i.e., the corn straw (both raw and torrefied shown on top rows of Fig. 2 and Fig. 3) varied a lot, hence the weight of these particles varied with their depth. This third dimension was challenging to photograph, as it was difficult to make such flakes stand upright under the microscope. As an example, the three torrefied corn straw particles shown in Fig. 2 had masses which did not directly correspond with their two shown dimensions. This was due to either differences in the third dimension of these flakes, i.e., their depth, and/or to difference in their densities. The photographs of each of those biomass particles at their initial states are shown in Fig. 2 and in Fig. 3, along with their mass. Sequences of six photographic snapshots from cinematography of the combustion of these individual raw and torrefied biomass particles are shown in Fig. 2 and in Fig. 3, respectively, along with their temperature histories.

3.2. Combustion temperatures and burnout times of individually-known particles

Combustion of both raw and torrefied biomass occurred in two distinguishable combustion phases (volatile matter flames and char oxidation); both were captured by concurrent pyrometry and high-speed cinematography, see Fig. 2 and Fig. 3. Capturing the flame temperature of the burning volatile matter of raw biomass particles pyrometrically was previously challenging in this laboratory during combustion of particles of small sizes (75–90 µm) [73,100]. This is because raw biomass particles form low-luminosity flames, as their devolatilization products contain mostly CO_2, CO, H_2 and light hydrocarbons that generate little soot in their envelope flames [51]. Thus, the brightness level of their envelope flames was low. As a result, in those studies the two distinct phases of the raw biomass particle combustion could only be detected by cinematography, not by pyrometry. However, the bigger (millimeter size) particles burned herein generated sufficiently strong signals to allow pyrometric detection. A number of the resulting complete temperature-time profiles of three selected particles from each type of biomass are shown in Figs. 2 and 3. Peak temperatures and overall burnout-times (both for the volatile matter flames and the chars) of all ten particles from each type of biomass burned herein are included in Table A1 of the Supplementary Material A; mean peak temperatures and burn out times of these ten individual particles, from each biomass type, are included in Fig. 4a and b, respectively.

For all particles from each type of biomass, shown in Fig. 2 and in Fig. 3 and included in Fig. 4, the peak volatile flame temperatures were in the range of 2100–2250 K. Flame temperatures of

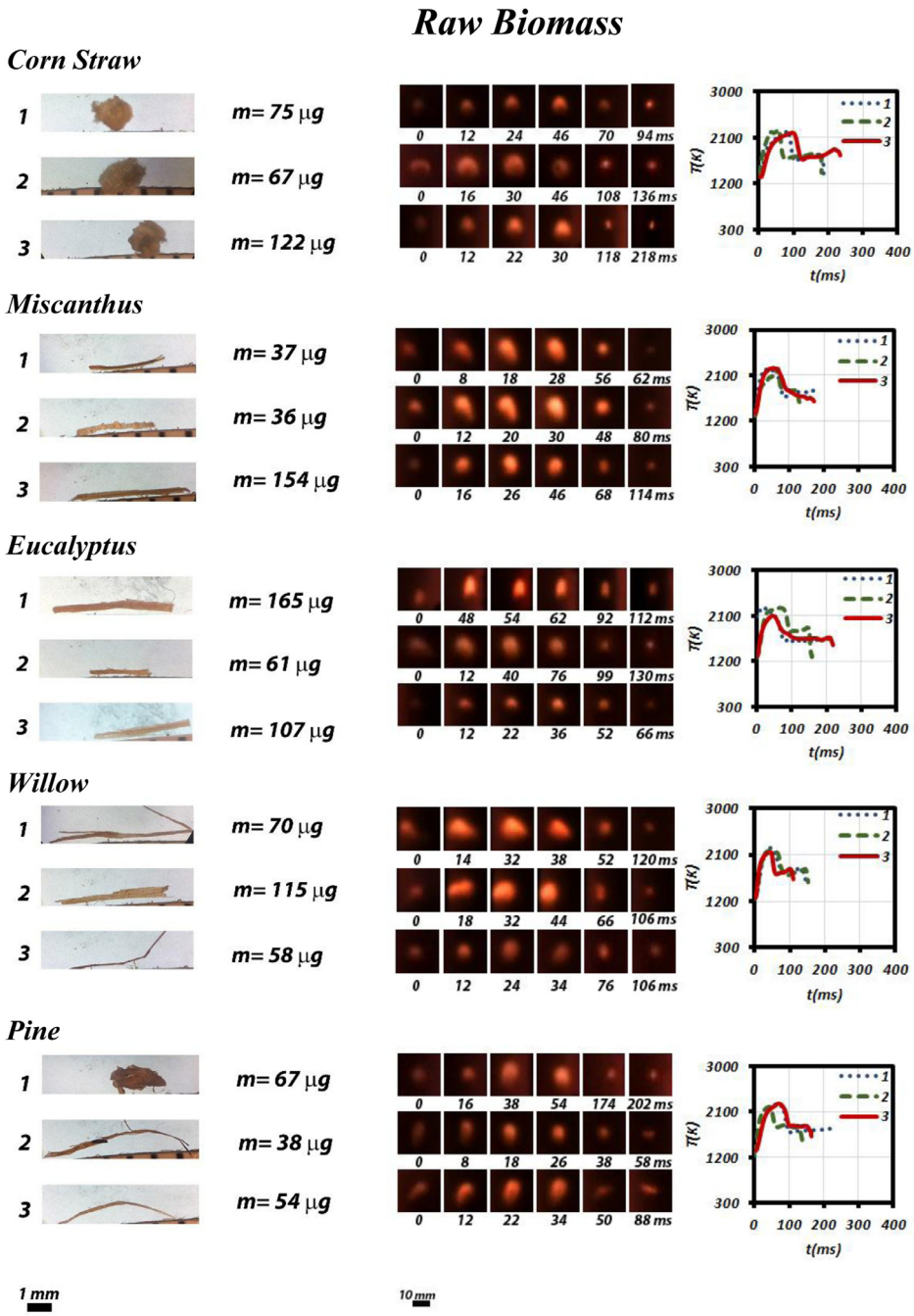

Fig. 2. Optical microscopy photographs of three individual particles of raw biomass along with their weights and selected snapshots of the combustion of three individual biomass particles captured with high-speed cinematography. Pyrometric temperature-time profiles are shown for each case. Pyrometric intensity, time and temperature of individual biomass particles are provided in the Supplementary Material B section.

torrefied biomass were 50–100 K higher than those of the raw biomass. This may be attributed to the different compositions of the combustible pyrolyzate gases. It has been reported that the biomass pyrolysis gas mainly contains CO_2, CO, CH_4, H_2, C_2H_6, C_2H_4, CH_3OH, C_3H_6O, minor amounts of higher gaseous organics and water vapor [101]. Raw biomass has higher moisture and oxygen content, hence its pyrolyzates gases are likely to contain more water vapor, which is a diluent, and more oxygenated hydrocarbons, combustion of which releases less heat. Based on these reasons, combustion of the raw biomass pyrolyzates attained lower flame temperatures than the torrefied biomass pyrolyzates. The peak char temperatures of raw and torrefied biomass were in the range of 1600–1800 K, which is a little lower as compared to char temperatures of different ranks of coal of considerably smaller size (75–90 µm) burning under identical conditions [100]. In a recent study in this laboratory, concerned with the selection of the particle size of torrefied biomass for co-firing with coal in power generation boilers, Panahi et al. [37] reported that char temperatures of torrefied biomass initially increased with increasing particle size, reached a maximum and thereafter decreased with further increasing particle size. The latter decreasing trend is typically attributed to diffusion-controlled burning of larger solid fuel particles as the diffusional reaction rate coefficient is inversely proportional to the particle diameter [102,103]. Char temperatures of torrefied biomass were 50–100 K lower than those of raw biomass. This discrepancy can be attributed to reasons related to both the physical and the

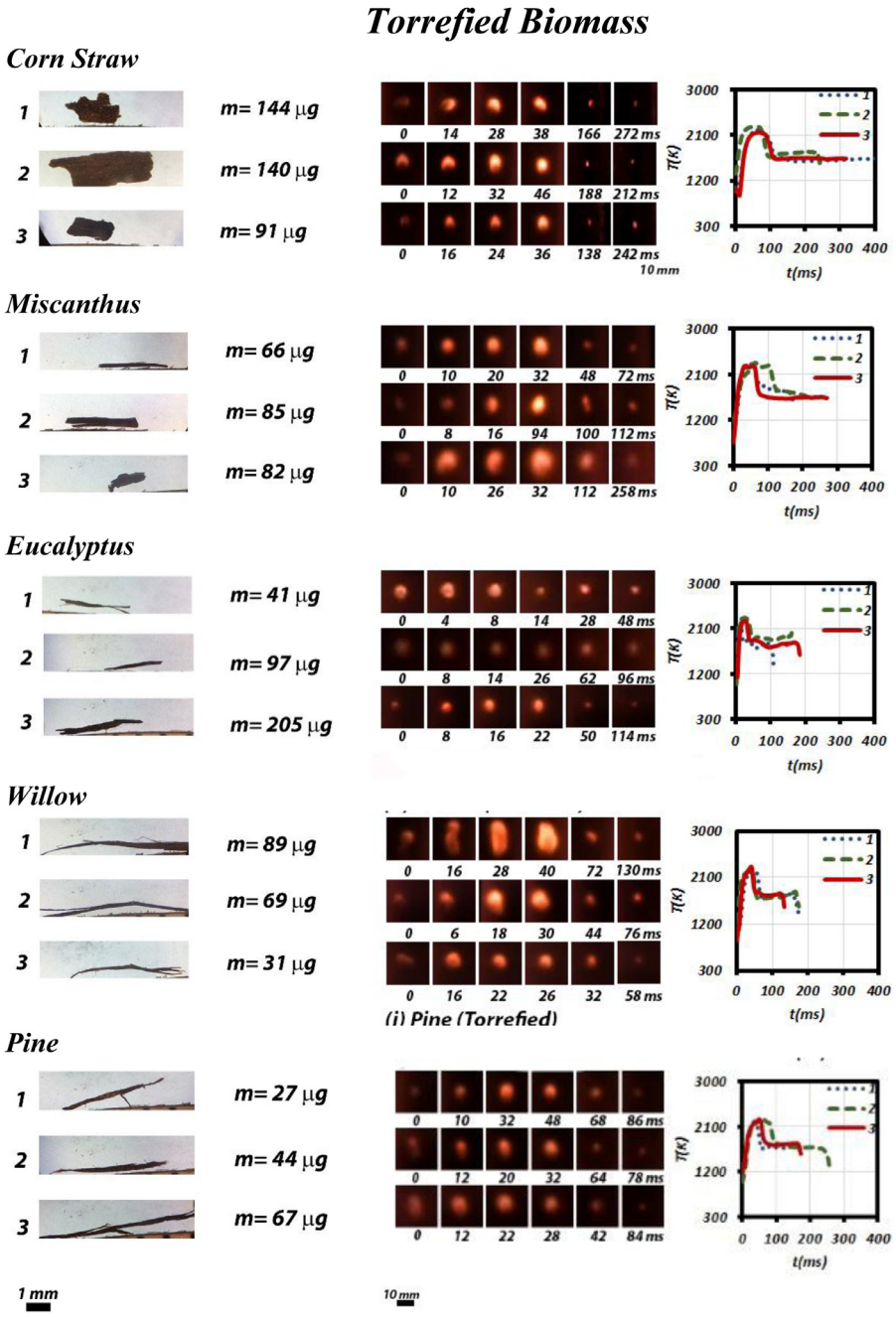

Fig. 3. Optical microscopy photographs of three individual particles of torrefied biomass along with their weights and selected snapshots of the combustion of three individual biomass particles captured with high-speed cinematography. Pyrometric temperature-time profiles are shown for each case. Pyrometric intensity, time and temperature of individual biomass particles are provided in the Supplementary Material B section.

chemical structures of the chars. The former includes aspect ratios, porosity, pore structure, etc., while the latter include elemental composition and (partial) decomposition of the chemical structures (hemicellulose, cellulose and lignin). Torrefied corn straw recorded the lowest char temperature among the rest, likely because of its physical and chemical structures [84], given that this biomass has the highest amount of ash among the types of biomass examined herein.

Burnout times of the volatiles and burnout times of the chars were directly obtained from pyrometric and cinematographic observations, and both were in good agreement. Total burnout times (volatile + char) of torrefied biomass were typically longer than those of raw biomass. Overall, the raw biomass particles burned for 110–218 ms; whereas the torrefied biomass particles burned for 140–233 ms. Raw biomass types typically have higher volatile matter mass fractions than their torrefied counterparts, with the exception of pine; thus, the combustion duration of their volatiles was longer, again with the exception of pine. Char burnout times of torrefied biomass were drastically longer than those of raw biomass because of their higher fixed carbon mass fractions. Raw Miscanthus has the lowest fixed carbon content and, therefore, it displayed the shortest char burnout duration. For all individually recorded particles (10 particles burned in each case), their photographs, masses, maximum lengths and maximum widths, measured flame and char combustion durations, as well as maximum deduced flame and char surface temperatures are listed in Table A1, which is included in Supplementary Material A.

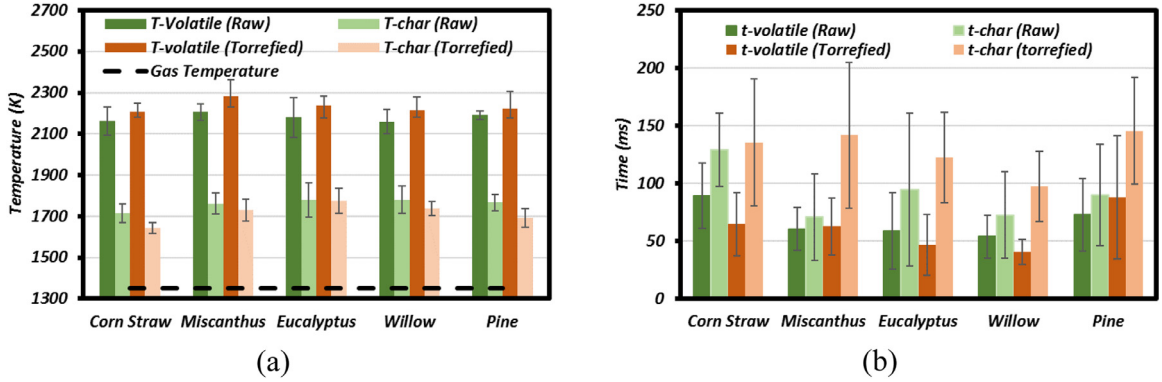

Fig. 4. Average (a) peak pyrometric temperatures and (b) burn-out times for the volatile and char combustion phases of the raw and torrefied biomass (10 particles in each case), burning in air, at T_{gas} = 1350 K.

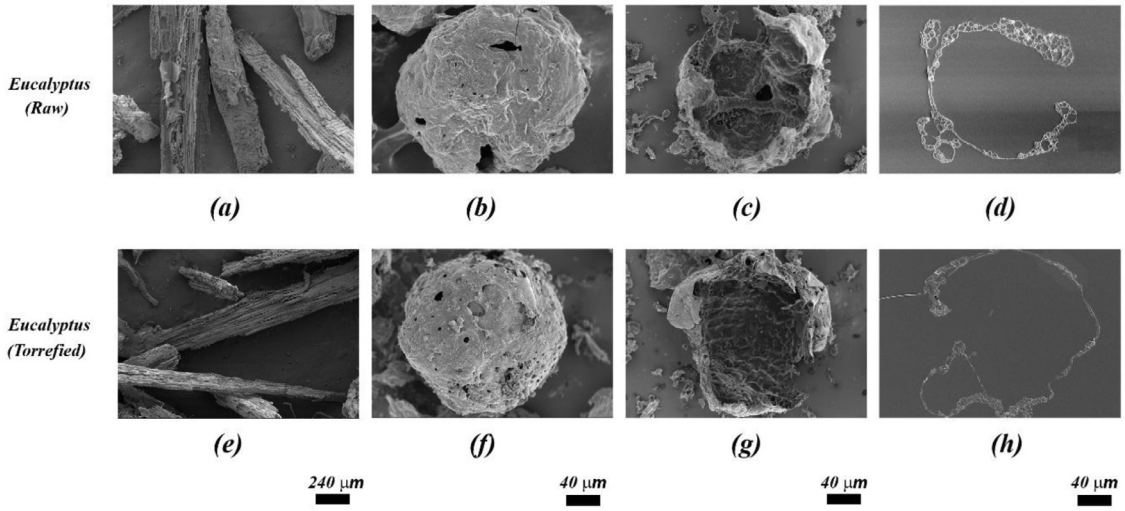

Fig. 5. Scanning Electron Microscope (SEM) photographs of original particles (*a* and *e*), and char particles (*b–d* and *f–h*) obtained from pyrolysis of raw and torrefied eucalyptus biomass particles (212–300 μm) in nitrogen, at a furnace wall temperature at T_{gas} = 1350 K. SEM was performed with a Hitachi S-4800 instrument, operated with a 3 kV of accelerating voltage, 10 μA of beam current and 8.5 mm working distance.

3.3. Structure, density and ash content of the chars

Since structural char parameters (morphology, porosity, density, etc.) of the particles burned in this study were not known a priori and could not be obtained in real time, additional experiments and kinetic phenomenological modeling were conducted to aid this investigation. Those experiments were conducted by pyrolyzing other biomass particles, collected by sieving in the size cut of 212–300 μm. These particles were overall smaller than those burned herein and, thus, they could be readily fluidized and introduced to the DTF in steady flow streams. Therein, they were pyrolyzed in nitrogen under conditions similar to those implemented during the combustion experiments (same furnace temperature, gas flow rate, and high heating rate – calculated to be 10^4 K s^{-1} from cinematographic recordings of particle ignition delay times in the furnace). The generated chars were collected on a paper filter at the exit of the DTF. Their microscopic examination by observation of SEM images of at least 20 particles per each sample provided a clear picture of the physical structural transformations of the biomass particles during pyrolysis and char formation. Scanning electron microscope (SEM) photographs of representative examples are shown in Fig. 5. Therein original eucalyptus wood particles are shown (*a*: raw and *e*: torrefied), their chars (*b*: raw and *f*: torrefied), as well as their char interiors (*c*: raw and *g*: torrefied). Moreover, char particles were embedded in epoxy and sectioned by a thin knife (*d*: raw and *h*: torrefied).

Thus, as Fig. 5 illustrates, that the char particles appear to be cenospheric and possess large cavities with thin walls. The fact that rapidly heated small biomass particles (where heat conduction to the particle interior is effective) undergo melting has already been reported for different types of biomass by Panahi et al. [89], Cetin et al. [60], Gill et al. [104], Reed and Williams [105], Lèdè et al. [106] and Narayan and Antal [107], Dall'Ora et al. [54], Maliutina et al. [108] among others. The particle structure and surface details of the char shown in Fig. 5 confirm recent findings of fusion and spherodization of biomass particles of sizes relevant to pulverized fuel combustion [89]. Similar physical transformations and formation of cenospheric chars were observed during high heating rate – high temperature pyrolysis of torrefied Willow and torrefied Eucalyptus biomass by McNamee et al. [109]. In terms of the biomass char shape, spherodization was pronounced for all of the torrefied biomass types examined herein, and for the raw miscanthus and raw eucalyptus biomass.

Furthermore, the bulk density of the collected biochar samples was measured by packing a small glass vial with char particles and tapping the vial by 100 taps [110]. The volume and weight of the packed bed were then measured, and the bulk density of the bed of biochar was calculated. The bulk densities of the

Table 2
Bulk biochar densities of the raw and torrefied biomass in this study.

Biochar	Herbaceous				Woody					
	Corn straw		Miscanthus		Eucalyptus		Willow		Pine	
	R	T	R	T	R	T	R	T	R	T
ρ_{bulk}[kg/m^3]	140±5	180±3	120±4	200±2	110±6	230±2	180±4	280±2	160±5	250±2

Table 3
Ash in high heating rate char, calculated volatile yield and volatile matter ratio.

Rank/fuel		Herbaceous biomass				Woody biomass					
		Corn straw		Miscanthus		Eucalyptus		Willow		Pine	
Content	Basis	R	T	R	T	R	T	R	T	R	T
Ash, wt%	dry	49.9	24.9	28.3	14.0	5.1	2.4	15.3	10.6	11.9	5.8
$\boldsymbol{VM_{ash\ tracer}}$, wt%	dry	92.5	78.5	93.8	88.6	94.6	86.5	94.2	84.9	95.4	75.6
VM ratio	–	1.23	1.19	1.16	1.12	1.30	1.11	1.25	1.11	1.29	0.93

σ_{ash}= ±0.3%; σ_{VM}= ±3.7%.

biochar samples that were examined herein were averaged over five experiments and the values are shown in Table 2. They are in the range of 110–280 kg/m^3. Such values are in line with values reported in the literature [111].

To determine the ash contents of the chars made in the laboratory, by pyrolyzing the biomass fuels in the DTF, the collected chars were burned in a thermogravimetric analyzer (TGA) at $T = 1000$ °C. The residual weight obtained after TGA combustion of the chars in air was recorded. Results for all types of biomass are listed in Table 3. Close examination of these results reveals that the ash contents of the chars are higher than the ash contents of the original biomass particles obtained from the Proximate Analysis at $T = 550$ °C, as listed in Table 1. Based on these ash values, the amounts of volatile matter (*VM*) released during high heating rate/high temperature devolatilization of biomass in the DTF can be calculated using the ash tracer technique [112] with Eq. (1), where α_0 represents the ash content of the original biomass sample and α_{char} represents the ash content of the char:

$$VM_{ash\ tracer} = \frac{\left(1 - \frac{a_0}{a_{char}}\right)}{\left(1 - \frac{a_0}{100}\right)} \tag{1}$$

Results for all types of biomass are reported in Table 3. The volatile yield calculated from the ash tracer technique will be used for the combustion rate analysis in the ensuing section. The fundamental assumptions of the ash tracer technique are that biomass ash is conserved within the char and that the ash fraction in the biomass is not affected by the time-temperature history of the particle. This assumes that ash species are not volatilized, or at least that the amount of volatilization which happens in the actual combustion experiment is the same as that which occurs under the conditions of this technique [113]. The volatile matter yield obtained from the experiments herein in the DTF by the ash tracer technique provides insight on the amount of condensed matter collected with the char residues or on the extent of vaporization of ash. The ash tracer technique for determination of the volatile yield, however, is more prone to errors introduced by selective losses of ash during particle collection [114].

The ratio of the volatiles obtained from the high heating rate experiments (ash tracer method) to those obtained from the Proximate analysis at low heating rates [115] is also called High Volatile Yield. It signifies the increased volatile release at high temperature high heating rate pyrolysis conditions. The volatile matter ratio can be calculated from equation below:

$$VM_{ratio} = \frac{VM\ (ash\ tracer\ method)}{VM\ (prox.\ analysis)} \tag{2}$$

The VM_{ratio} from pyrolysis in the DTF at the given temperatures is listed in Table 3. The results show that pyrolysis in the DTF leads to an expected increase in ash content in char, and to increased volatile yields as well. The only sample which does not follow this trend is the torrefied pine sample. Ash contents of the torrefied biomass chars are lower than those of raw biomass chars. A potential explanation is the loss of reactive volatile species due to breakage of the weakest bonds and loss of light volatile compounds during torrefaction. This would shift the formation of pyrolysis products to heavier species and favor a coking process, which Zheng et al. [116] have reported for torrefaction conditions similar to those implemented herein. This, in turn, would reduce the volatile loss and increase the char formed during pyrolysis. Accordingly, the VM_{ratio} is lower for all torrefied biomass chars compared to their raw biomass counterparts. For pine, the torrefied biomass char sample even shows a VM_{ratio} that is less than unity, which is still in agreement with the notion that cross-linking processes may have occurred.

It should be mentioned here that ash tracer measurements on biomass samples are always challenging, as reported by Liaw and Wu [117]. It is a given fact that many of the ash components are volatile (alkali and earth alkali metals), and that the low ash content in general is a problem when experiments with diminutive sample mass, as in this case, are carried out. One may argue that a longer sampling time for smaller particles is the solution to collect enough char to carry out a detailed ash composition analysis, which can also provide results on thermally stable components. However, in this case the primary target is the investigation of single particles. Thus, whereas a detailed ash analysis gives good information on a bulk sample (by collecting small size char or ash particles over a long time), individual particles may still be affected by particle-to-particle variations to a large degree. It must be noted, that using the ash tracer method is associated to certain difficulties, especially in the case of biomass. Many biomass samples contain ash species which are volatile at combustion temperatures, e.g. Na, K and Ca. Some authors suggest to use single ash species [118] or even use an integral method which samples the solid from pyrolysis/combustion completely, such that a mass balance between reactor input and output can be used to determine the volatile loss by difference [117]. Although such a method would be beneficial, its use in the given case is limited as the burnout data stems from single particles, which may vary in their ash and char contents from particle to particle. Both facts, the volatility of ash species and the particle to particle variability, may have an impact on precise numbers for char yield, which will directly affect the char mass and, thus, the char particle diameter

which is proportional to $m_{char}^{1/3}$. As the particle-to particle variability is a primary effect which cannot be cancelled out in the given experiment, the uncertainty in ash content due to ash volatility has to be kept in mind but it is not considered directly in this work.

4. Phenomenological modeling of biomass char combustion

Phenomenological modeling was conducted herein for all of the individually-recorded biomass particles of Figs. 2 and 3, both raw and torrefied, to investigate the physical characteristics of their chars and obtain their burning rates. The experimental data showed that the char burning phase lasts longer than the volatile combustion phase, although the particle mass is dominated by the volatile matter; see Table 3. Based on the pyrometric and cinematographic observations, it was not entirely clear what was the structure of the char residue upon termination of the devolatilization stage. To apply the numerical model knowledge of the structural transformation details of the chars was necessary. The following steps were taken to separate the char conversion phase of each individual particle and apply a char combustion model on the collected pyrometric data of the previous section:

1. The char combustion phase was separated from the complete pyrometric temperature profile of each particle. The transition from volatile to char combustion was defined as the point when the volatile temperature peak had decreased to a minimum.
2. The char temperature profile, which was measured with a temporal resolution $\Delta t \cong$ 17 µs (i.e. 10,000 T_p-t pairs for a char particle with 100 ms char burnout time), was smoothed using a 6th order polynomial and Δt was reduced to 1 ms, making the applied fitting routine much more time-efficient.
3. The char burnout was modeled by tracing the measured temperature profile and assuming the necessary fuel specific parameters from Tables 2 and 3.

Char conversion modeling is often based on the solution of the energy balance around burning char particles with T_p and d_p as input parameters from pyrometry, as has been described in [79]. However, as the model was initially designed for fitting Arrhenius parameters to multi-particle T_p-d_p averages, a modification of the equations and of the fitting scheme, respectively, was undertaken. To begin with, the mass of the char particle m_p after completed pyrolysis is needed to track its burnout over time. The mass of the char particle, m_p, was obtained from the measured mass of its parent biomass particle, $m_{biomass}$, by using the Eq. (3):

$$m_p = m_{biomass}(1 - VM_{ash\ tracer}) - m_{ash} \tag{3}$$

Contributions come from the ash content (Table 1) and the volatile content obtained from the high heating rate experiments in the DTF (Table 3). The burning rate calculation requires information on the char temperature T_p at $t = t_0$ and on the char diameter d_p. As the typical char particle is expected to be highly porous and cenospheric (see Fig. 5), d_p needs to be calculated based on the assumption that the char particle mass is concentrated in a carbon rich shell enveloping the internal void of the cenosphere. Assuming that the cenospheric char particles have a highly porous and thin wall and a large internal void, their external diameters are calculated from the equation below:

$$d_p = \sqrt[3]{\frac{6}{\pi}\frac{m_p}{\rho}\cdot\frac{1}{(1-\varphi)}} \tag{4}$$

where φ is the particle porosity, and ρ is the apparent density. With measured T_p and calculated d_p, the energy balance at $t = t_0$ can be solved according to [79], as shown in the equation below:

$$\underbrace{\varepsilon\sigma\left(T_p^4 - T_w^4\right)}_{radiation} + \underbrace{\frac{2\lambda}{l^*}\left[\frac{\frac{\kappa}{2\gamma}}{\exp\left(\kappa\ \frac{A_p}{\gamma l^* F^*}\right) - 1}\right](T_p - T_g)}_{convection} = \underbrace{\frac{\dot{n}_c \Delta h}{A_p}}_{reaction} + \underbrace{\frac{V_p}{A_p}\rho_{app} c_p \frac{dT_p}{dt}}_{thermal\ inertia}, \tag{5}$$

The quantity $\kappa = \dot{n}_c^p \gamma l^* \sum^{\nu_i} c_{gi}/\lambda$ is a modified Péclet number and expresses a decrease of the convective heat transfer caused by the non-equimolar heterogeneous reaction on char surface producing either CO or CO_2. The coefficient $\gamma = (\psi - 1)/(\psi + 1)$ depends on the (CO/CO_2) production ratio $\psi = 0.02\exp(-3070/T_p)p_{O_2,s}{}^{0.21}$ in the global reaction: $C(s) + (\frac{1+\psi}{2})O_2 \rightarrow \psi CO_2 + (1-\psi)CO$, and the stoichiometric coefficients ν_i are calculated based on that assumption. The parameter l^* is the characteristic length of the particle and $p_{O_2,s}$ is the oxygen partial pressure on the particle surface. Note, that this model has been developed for both spherical and non-spherical biomass particles, as described in [79]. Therein, l^* and F^* are parameters describing the shape of prolate biomass particles. In the given case, these shape-dependent parameters are chosen for spherical particles, as the results from the SEM shown in Fig. 5 indicate this shape to be appropriate. According to the non-equimolar mass transfer in the boundary layer, the oxygen partial pressure at the particle surface (including Stefan flow effects) reads as

$$p_{O_2,s} = \frac{p}{\gamma} + \left(p_{O_2,\infty} - \frac{p}{\gamma}\right)\exp\left(\frac{\psi - 1}{2}\frac{\dot{n}_C^p}{D_{O_2}}\frac{A_p}{F^*}\frac{RT}{p}\right). \tag{6}$$

Solving Eqs. (5) and (6) at $t = t_0$, the instantaneous burning rate $\dot{n}_C^p$ is calculated, and the mass of the char particle at time step t_{i+1} is given as:

$$m(t_{i+1}) = m(t) - \dot{n}_C^p A_{ext}\mu_c \Delta t, \tag{7}$$

which is based on the mass of the current time step, the external surface A_{ext}, the molar mass of carbon μ_c and the time step Δt. As a consequence, the external particle diameter shrinks (assuming boundary diffusion to be dominating, zone III [119]) when the result of Eq. (7) is inserted in Eq. (4). With the new $d_p(t_{i+1})$, $m_p(t_{i+1})$ and $T_p(t_{i+1})$ taken from the experimentally determined temperature profile the values for the next time step are updated. This is repeated until either all the carbon gets consumed and the particle mass equals the ash content, or the temperature profile of the particle ends without reaching complete burnout.

This char burnout model, which considers the cenospheric shape of particles, was first tested against the synthetic carbonaceous ash-free cenospheres of Levendis and Flagan [87], a well-characterized ash-free material which seems to be most suitable for these tests as it contains neat carbon and has similar shape to most of the investigated biomass char particles of this study. These cenospheres, that have diameters in the narrow range of 150 to 175 µm, were burned in the drop tube reactor under similar thermal conditions at 100% O_2. The particle structure, in particular the thin wall shell which includes significant large pores, is shown in Fig. 6. The density of the shell was taken to 1400 kg/m³, a value below the reported 1800–2000 kg/m³ (measured with helium porosimetry) in the given reference. The reason is the clear occurrence of large “blow holes” during high-heating rate pyrolysis which, in essence, reduce the mass of the cenosphere. In the model this reduction of mass was accounted for by changing the char density and keeping its diameter and thickness constant. Furthermore, it has to be considered that the cross-sections not neces-

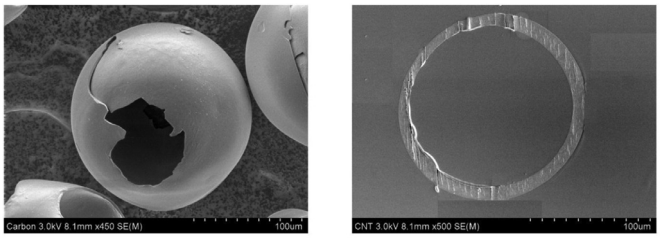

Fig. 6. SEM images of a synthetic carbon cenosphere [87], and a cross section of another carbon cenosphere embedded in epoxy and then sliced with a small diamond knife.

sarily cut through the equator of the particle, which can make the shells appear thicker than in the real particle by angular effects.

Based on the SEM images the porosity φ (i.e., the internal void) of the particles was estimated to be φ= 0.9. With an average particle diameter of such cenospheres taken as 165 µm, the calculation of the burning rate along the temperature trajectory was carried out. The results, representing 97–99% burnout for the three particles, are shown in Fig. 7. The comparison of the model to these more precisely characterized ash-free particles shows the capability of the model to describe the combustion in the given case of cenospheric particles.

Next, attention was turned to the biomass char particles. Figure 8 shows examples for char combustion of three biomass particles (raw Eucalyptus particle #2, raw Miscanthus particle #2 and torrefied Willow particle #2); the rest of the particles of Figs. 2 and 3 are included in the Supplementary material C. The diagrams show a correlation between burning rate and particle temperature as expected. For the Miscanthus and Willow char particles, the clear temperature drop at the end indicates that the particle has lost major parts of its carbon content and the assumption of complete burnout is justified. The Eucalyptus particle shows a similar trend, but not as evident as for the other two particles. While burnout is increasing nearly-linearly, the combustible (char) part of the particle mass decreases in the same way.

The temperature plots demonstrate the variations in char temperature for these particles, which have been smoothened for simplifying the burning rate computations. Most of the parameters of Eqs. (3)–(7) are available from different analyses and are presented in Tables 1–3. As most of the char particle porosity is assumed to be caused by a central void in the particle, only a thin carbonaceous shell needs to be consumed. Note, that actual particles still have smaller pores in their carbon shells, which makes the real shell thickness slightly bigger than the computed one. The inner diameter of this void was calculated from the equation below:

$$d_{p\ inner} = \sqrt[3]{\varphi} d_p \tag{8}$$

All particles with complete temperature profiles were subjected to the same fitting routine. The missing parameter of porosity φ was varied for each particle to reach a carbon conversion of at least 99% of the char, leaving only ash. This was carried out successfully for all biomass char particles. Plotting the resulting best fit porosity against the initial char diameter which has been calculated according to Eq. (4) leads to the results plotted in Fig. 9a. They show that many of the investigated particles require high porosities (i.e., large central voids) to achieve complete burnout under the given conditions.

It must be noted that combustion primarily took place under diffusion-limited (zone III) conditions, mainly an initial heating phase and the end phase with decreasing temperature were subject to zone II (pore-diffusion limited) combustion. The high porosity of the chars causes a large inner diameter $d_{p\,inner}$ and thus a large outer diameter d_p, which increases the total carbon consumption rate.

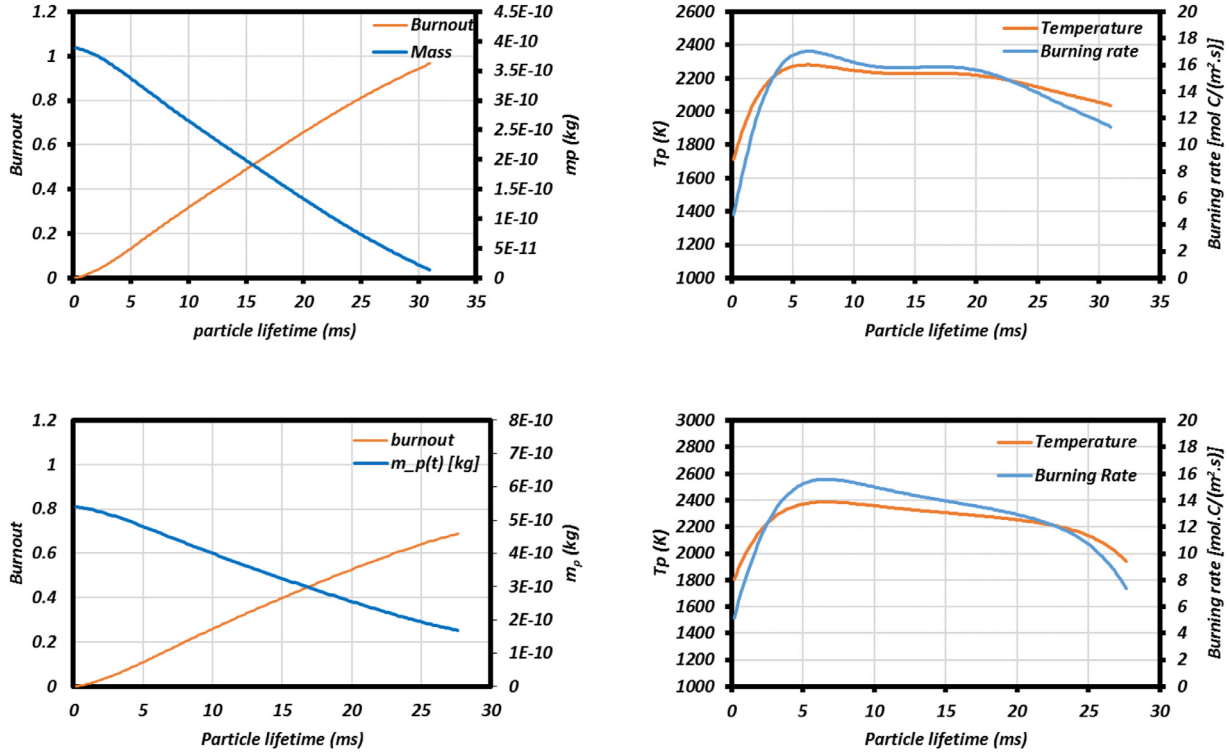

Fig. 7. Time dependent profiles of particle burnout, particle mass, experimental temperatures and deduced burning rates for combustion of two synthetic carbonaceous cenospheres in 100% oxygen.

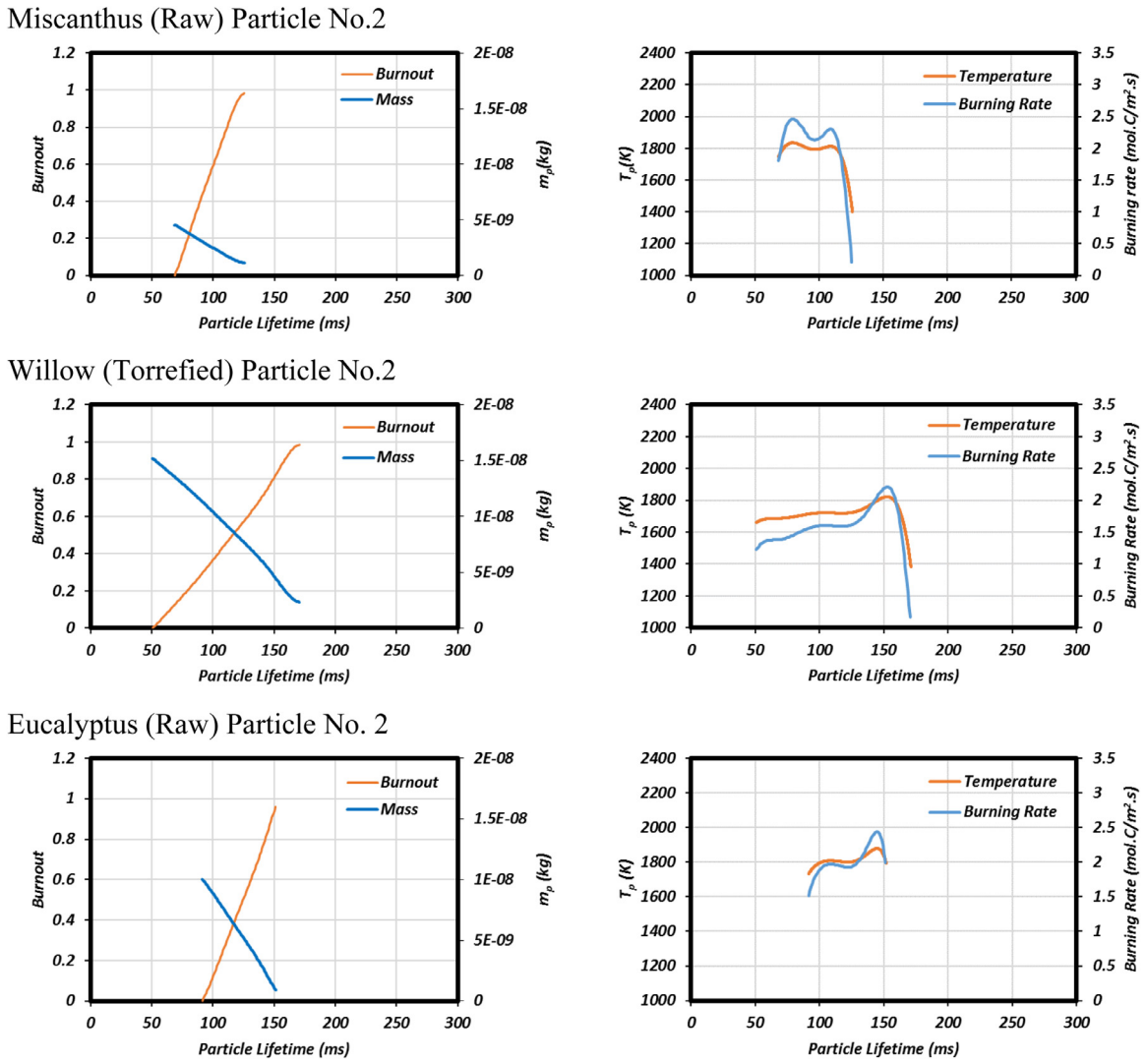

Fig. 8. Particle mass and char burnout (left column) and fitted particle temperature with the burning rate of carbon for (a) Miscanthus (Raw) Particle No. 2, (b) Willow (Torrefied) Particle No. 2 and (c) Eucalyptus (Raw) Particle No. 2.

Figure 9b shows the dependency of porosity on initial char density. It shows that lower density char requires a smaller void to achieve burnout, although raw Eucalyptus and raw Miscanthus do not fit into this tendency precisely. All chars with an apparent density above 180 kg/m³ require very high porosity (larger void) to reach a sufficient burnout level; a lower porosity (smaller void) would mean incomplete burnout. Additional parameters which were tested for their influence on the required porosity are volatile content (Fig. 9c) and initial char mass (Fig. 9d). The former shows a weak tendency to require lower porosity with higher volatile content, while the latter seems to show a tendency to reduced porosity with lower char mass.

The results of the burnout fits need some discussion:

Considering the porosity, which is equal to the void diameter for the assumed cenospheric particles, 80% of all particles which are listed in Fig. 9 have $\varphi > 0.8$, which corresponds to relative shell thickness $s = \frac{d_p - d_{p\ inner}}{2} = 0.93$, that seems to be rather low for a stable shell. However, all burnout predictions showed that with lower porosity, and thus lower particle diameter, incomplete burnout would be the consequence. The same effect occurred for the assumption of homogeneous porosity, which causes a strong decrease in particle diameter, but also fails to reach high conversion.

The single-particle observation approach itself is very detailed on one-hand, but causes some uncertainties on the other hand. Volatile and ash contents of the individual particles are uncertain as these values were obtained from batches of particles, in which the number and total mass of particles help to reduce particle-specific outliers. The single particles might not follow this trend particle by particle. However, the trend to incomplete burnout for lower porosity and/or considering sponge-like structures instead of cenospheres, was very clear in the modeling. It can be concluded that while such variations need to be kept in mind, the general fact that the particle wall structure has a dominant influence is not affected by these uncertainties.

In literature a few examples of biomass char analysis by SEM are given which show that these structures have been observed in other experiments as well [61,89,120]. Trubetskaya et al. [57] showed that pine and wheat straw has a clear tendency to form such thin shells. Senneca et al. [121] reported thin carbonaceous walls for Walnut shell chars. The authors are not aware of any study which has quantified the resulting shell thickness of biomass chars which show a tendency to softening and metaplast formation, however the cross-sectional images of pyrolyzed pine char in [60] and the detailed reviews of Yu et al. [122] and Wall et al. [123], both on coal chars, show that porosities above

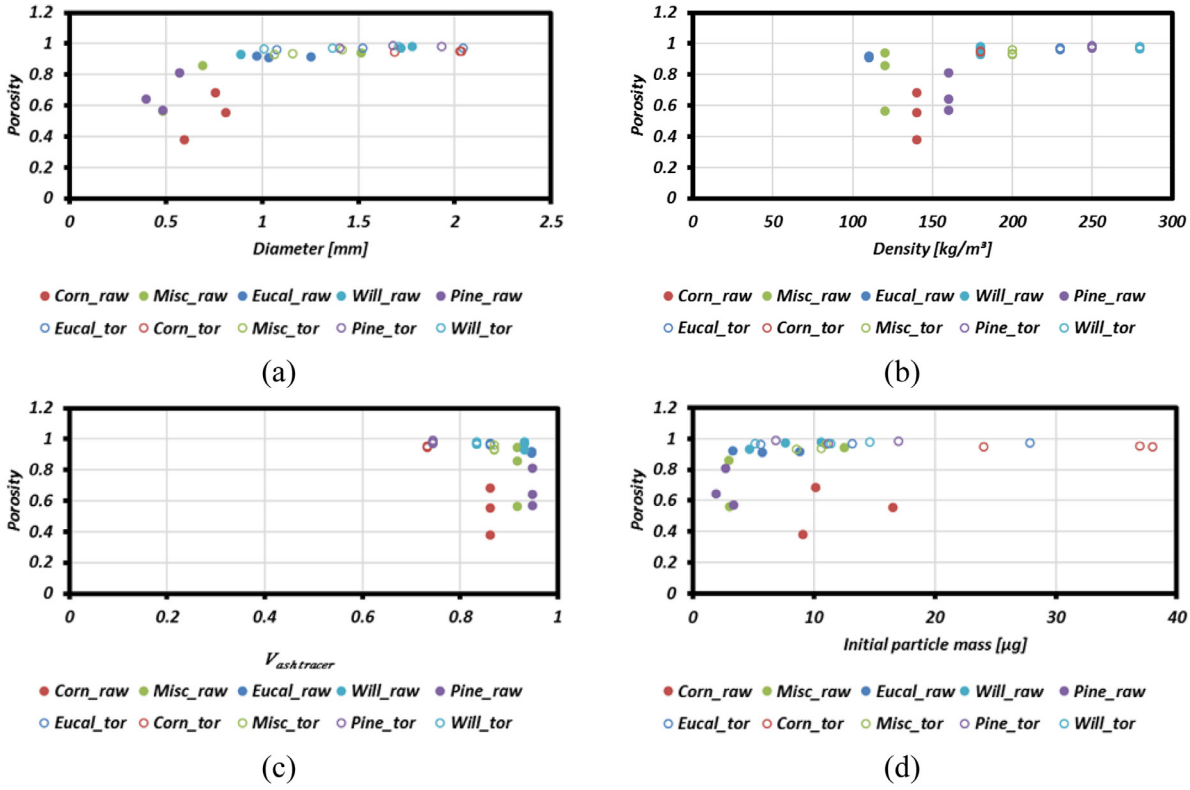

Fig. 9. Best-fit porosity plotted against (a) initial char diameter, (b) apparent char density, (c) the volatile content of the biomass samples and (d) the initial char mass.

80% and walls with less than 5 µm thickness are still stable and existent.

The high volatile content ($VM_{ratio} \geq 73\%_{dry}$ according to Table 3) leads to the assumption that small inaccuracies in char burnout calculations cause acceptable uncertainty in complete utilization of the energy supplied by each of the fuels. However, the ash quality might suffer if excessive unburned carbon is left. Therefore, modeling of char burnout merits deeper investigation for those types biomass fuel particles which undergo the previously observed phenomenon of spherodization [54,57,89] and the formation of cenospheric char particles, as is reported for most of the biomass types of this study. A set of experiments which combines the direct observation of particle mass and dimensions with burning times, temperature (and preferably diameter) profiles and precise measurement of carbon content at the end of the temperature trajectory would be a solution to reach higher accuracy in modeling trajectories and identifying relevant factors to describe burnout times precisely. As the current experiment made it impossible to capture the ash after combustion of each individual particle, this step is still left for further work. However, ashes were collected from additional experiments with smaller biomass particles (212–300 µm), which were easily fluidized in streams (as mentioned in Section 3.3) and then were either pyrolyzed or burned in the DTF. Figure 10 shows an SEM photograph of a number of burned out particles of raw eucalyptus. Most of the ash particles appear to be spheroidal in shape, with dimensions in the neighborhood of 150 µm.

Overall, this work illustrates the significance of the char structure for high resolution modeling approaches, such as direct numerical simulation (DNS) or Large Eddy Simulation (LES) of pulverized fuel flames. Modeling of biomass needs to consider that char are likely to be cenospherical. For complete utilization and predictive modeling, which is nowadays an important topic

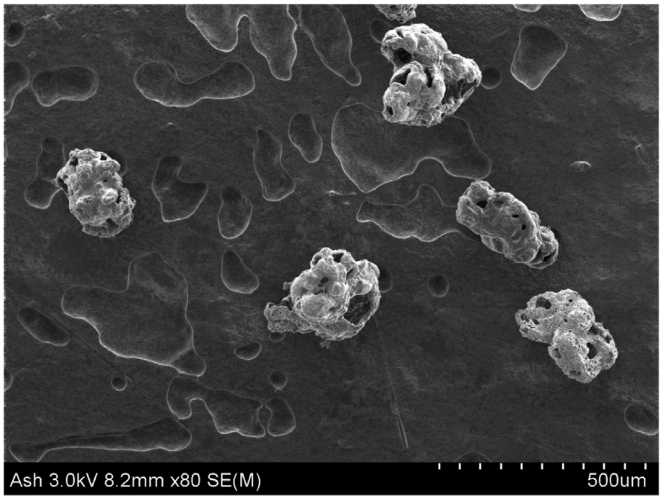

Fig 10. Scanning Electron Microscope (SEM) photographs of ash particles obtained from combustion of raw eucalyptus biomass of initial size in the range of 212–300 µm. Combustion occurred in air at a furnace temperature at $T_{wall} = 1400$ K.

[124–127], this result will be important to get a good description of char combustion.

5. Conclusions

A unique approach and methodology was implemented to determine the predominant char structure from detailed results of the combustion histories of biomass particles exposed to high temperatures at high heating rates. The particles were sufficiently small to be of interest to combustion in pulverized fuel boilers

[128] and, conversely, the particles were sufficiently large for their initial mass to be measured with a microbalance. This work also includes a detailed data set which has not been available before. This data set, besides the combustion behaviors of the individually-recorded raw and torrefied biomass particles, contains corresponding combustion behaviors of well-characterized synthetic carbonaceous cenospheres. The latter were used to validate a phenomenological model before it was applied to unravel the combustion of the biochars of the former. Furthermore, the theoretical analysis of the results gives deeper insight into pulverized biomass char combustion and allows recommendations for char combustion modeling.

This work burned individually weighted particles of several types of biomass (both raw and torrefied) and observed their combustion history. For each individual particle, the combustion history was recorded in real time with concurrent optical pyrometry and high-speed cinematography.

- Combustion details of the raw and the torrefied biomass particles were obtained documenting both their temperatures and their burn-out times.
- Physical details of the raw and torrefied biomass chars were investigated (density, shape, structure, porosity and size) by combining experimental data with phenomenological modeling.
- It was determined that biomass chars, generated under very high heating rates and high temperatures were typically cenospheric with thin and porous walls. The model applied to the particles gives a clear indication that the frequently observed cenospheric structure of biomass particles being pyrolyzed at high heating rates has to be considered in char burnout modeling. Future work can deal with investigating the porosity of the cenosphere walls, which is the next level of detail that can be found. Experimental work should concentrate on reducing the uncertainties in volatile and ash measurements, which is a time-consuming but revealing step to investigate the effects of particle structure.

Acknowledgment

This work was supported partially by the US National Science Foundation Grant # 1810961 and partially by the Deutsche Forschungsgemeinschaft (DFG, German Research Foundation) – Projektnummer 215035359 – TRR 129. The authors would like to thank Dr. Patrick Mason at University of Leeds for his assistance in conducting the proximate and ultimate analysis of the fuels.

Supplementary material

Supplementary material associated with this article can be found, in the online version, at doi:10.1016/j.combustflame.2019.06.009.

References

[1] B. Dudley, BP Energy Outlook 2030, (2013).
[2] F. Schipfer, L. Kranzl, D. Leclère, L. Sylvain, N. Forsell, H. Valin, Advanced biomaterials scenarios for the EU28 up to 2050 and their respective biomass demand, Biomass Bioenergy 96 (2017) 19–27.
[3] A. Brosowski, D. Thrän, U. Mantau, B. Mahro, G. Erdmann, P. Adler, W. Stinner, G. Reinhold, T. Hering, C. Blanke, A review of biomass potential and current utilisation–Status quo for 93 biogenic wastes and residues in Germany, Biomass Bioenergy 95 (2016) 257–272.
[4] IEA, CO2 emissions from fuel combustion highlights 2015, (2015).
[5] J. Rogelj, M. Den Elzen, N. Höhne, T. Fransen, H. Fekete, H. Winkler, R. Schaeffer, F. Sha, K. Riahi, M. Meinshausen, Paris agreement climate proposals need a boost to keep warming well below 2 c, Nature 534 (2016) 631.
[6] R. Lueken, K. Klima, W.M. Griffin, J. Apt, The climate and health effects of a USA switch from coal to gas electricity generation, Energy 109 (2016) 1160–1166.
[7] EIA, EIATotal energy data, (2017).
[8] Y.A. Levendis, A. Panahi, E. Rokni, X. Ren, Emissions from cofiring coals, in: B.A. Sakkestad (Ed.), 40th International Technical Conference on Clean Coal & Fuel Systems, Clearwater, Florida, USA (2015), pp. 533–544.
[9] J.L. Easterly, M. Burnham, Overview of biomass and waste fuel resources for power production, Biomass Bioenergy 10 (1996) 79–92.
[10] K. Hein, J. Bemtgen, EU clean coal technology—co-combustion of coal and biomass, Fuel Process. Technol. 54 (1998) 159–169.
[11] S.K. Sirumalla, A. Panahi, A. Purohit, A. Baugher, Y.A. Levendis, R.H. West, Nitrogen oxide evolution in oxy-coal combustion, US Eastern States Section of the Combustion Institute, 2018.
[12] R. Birley, J. Jones, L. Darvell, A. Williams, D. Waldron, Y. Levendis, E. Rokni, A. Panahi, Fuel flexible power stations: utilisation of ash co-products as additives for NO_x emissions control, Fuel 251 (2019) 800–807.
[13] A. Panahi, S.K. Sirumalla, R.H. West, Y.A. Levendis, Temperature and oxygen partial pressure dependencies of the coal-bound nitrogen to NO_x conversion in O_2/CO_2 environments, Combust. Flame 206 (2019) 98–111.
[14] M. Sami, K. Annamalai, M. Wooldridge, Co-firing of coal and biomass fuel blends, Prog. Energy Combust. Sci. 27 (2001) 171–214.
[15] A. Williams, M. Pourkashanian, J. Jones, Combustion of pulverised coal and biomass, Prog. Energy Combust. Sci. 27 (2001) 587–610.
[16] R. Backreedy, L. Fletcher, J. Jones, L. Ma, M. Pourkashanian, A. Williams, Co–firing pulverised coal and biomass: a modeling approach, Proc. Combust. Inst. 30 (2005) 2955–2964.
[17] A. Toptas, Y. Yildirim, G. Duman, J. Yanik, Combustion behavior of different kinds of torrefied biomass and their blends with lignite, Bioresour. Technol. 177 (2015) 328–336.
[18] J.P. Smart, R. Patel, G.S. Riley, Oxy-fuel combustion of coal and biomass, the effect on radiative and convective heat transfer and burnout, Combust. Flame 157 (2010) 2230–2240.
[19] E. Rokni, A. Panahi, X. Ren, Y.A. Levendis, Reduction of sulfur dioxide emissions by burning coal blends, J. Energy Resour. Technol. 138 (2016) 032204.
[20] E. Rokni, A. Panahi, X. Ren, Y.A. Levendis, Curtailing the generation of sulfur dioxide and nitrogen oxide emissions by blending and oxy-combustion of coals, Fuel 181 (2016) 772–784.
[21] E. Rokni, X. Ren, A. Panahi, Y.A. Levendis, Emissions of SO_2, NO_x, CO_2, and HCl from Co-firing of coals with raw and torrefied biomass fuels, Fuel 211 (2018) 363–374.
[22] A. Panahi, M. Tarakcioglu, Y.A. Levendis, Torrefied biomass size for combustion in existing Boilers, 10th US National Combustion Meeting (2017).
[23] R. Pentananunt, A.M. Rahman, S. Bhattacharya, Upgrading of biomass by means of torrefaction, Energy 15 (1990) 1175–1179.
[24] M. Van der Stelt, H. Gerhauser, J. Kiel, K. Ptasinski, Biomass upgrading by torrefaction for the production of biofuels: a review, Biomass Bioenergy 35 (2011) 3748–3762.
[25] A. Trubetskaya, P.A. Jensen, A.D. Jensen, A.D.G. Llamas, K. Umeki, D. Gardini, J. Kling, R.B. Bates, P. Glarborg, Effects of several types of biomass fuels on the yield, nanostructure and reactivity of soot from fast pyrolysis at high temperatures, Appl. Energy 171 (2016) 468–482.
[26] L.L. Baxter, T.R. Miles, B.M. Jenkins, T. Milne, D. Dayton, R.W. Bryers, L.L. Oden, The behavior of inorganic material in biomass-fired power boilers: field and laboratory experiences, Fuel Process. Technol. 54 (1998) 47–78.
[27] R. Zanzi Vigouroux, D. Tito Ferro, A. Torres, P. Beaton Soler, E. Björnbom, Biomass torrefaction, 2nd World Conference on Biomass for Energy, Industry and Climate Protection, 10-14 May 2004, Rome, Italy (2004), pp. 859–862.
[28] T. Keipi, H. Tolvanen, L. Kokko, R. Raiko, The effect of torrefaction on the chlorine content and heating value of eight woody biomass samples, Biomass Bioenergy 66 (2014) 232–239.
[29] T. Bridgeman, J. Jones, I. Shield, P. Williams, Torrefaction of reed canary grass, wheat straw and willow to enhance solid fuel qualities and combustion properties, Fuel 87 (2008) 844–856.
[30] D. Agar, M. Wihersaari, Bio-coal, torrefied lignocellulosic resources–key properties for its use in co-firing with fossil coal–their status, Biomass Bioenergy 44 (2012) 107–111.
[31] R.B. Bates, A.F. Ghoniem, Biomass torrefaction: modeling of volatile and solid product evolution kinetics, Bioresour. Technol. 124 (2012) 460–469.
[32] R.H. Ibrahim, L.I. Darvell, J.M. Jones, A. Williams, Physicochemical characterisation of torrefied biomass, J. Anal. Appl. Pyrolysis 103 (2013) 21–30.
[33] M.J. Prins, K.J. Ptasinski, F.J. Janssen, Torrefaction of wood: part 2. Analysis of products, J. Anal. Appl. Pyrolysis 77 (2006) 35–40.
[34] B. Arias, C. Pevida, J. Fermoso, M.G. Plaza, F. Rubiera, J. Pis, Influence of torrefaction on the grindability and reactivity of woody biomass, Fuel Process. Technol. 89 (2008) 169–175.
[35] V. Repellin, A. Govin, M. Rolland, R. Guyonnet, Energy requirement for fine grinding of torrefied wood, Biomass Bioenergy 34 (2010) 923–930.
[36] J. Jones, T. Bridgeman, L. Darvell, B. Gudka, A. Saddawi, A. Williams, Combustion properties of torrefied willow compared with bituminous coals, Fuel Process. Technol. 101 (2012) 1–9.
[37] A. Panahi, M. Tarakcioglu, M. Schiemann, M. Delichatsios, Y.A. Levendis, On the particle sizing of torrefied biomass for co-firing with pulverized coal, Combust. Flame 194 (2018) 72–84.
[38] E. Rokni, A. Panahi, Y.A. Levendis, Formation of acid gases from co-firing of coal with raw and torrefied biomasses, 10th US National Combustion Meeting (2017).
[39] P.A. Bejarano, Y.A. Levendis, Single-coal-particle combustion in O_2/N_2 and O_2/CO_2 environments, Combust. Flame 153 (2008) 270–287.

[40] J. Riaza, R. Khatami, Y.A. Levendis, L. Álvarez, M.V. Gil, C. Pevida, F. Rubiera, J.J. Pis, Single particle ignition and combustion of anthracite, semi-anthracite and bituminous coals in air and simulated oxy-fuel conditions, Combust. Flame 161 (2014) 1096–1108.
[41] R. Khatami, C. Stivers, Y.A. Levendis, Ignition characteristics of single coal particles from three different ranks in O_2/N_2 and O_2/CO_2 atmospheres, Combust. Flame 159 (2012) 3554–3568.
[42] T. Maffei, R. Khatami, S. Pierucci, T. Faravelli, E. Ranzi, Y.A. Levendis, Experimental and modeling study of single coal particle combustion in O_2/N_2 and oxy-fuel (O_2/CO_2) atmospheres, Combust. Flame 160 (2013) 2559–2572.
[43] B. Goshayeshi, J.C. Sutherland, A comparison of various models in predicting ignition delay in single-particle coal combustion, Combust. Flame 161 (2014) 1900–1910.
[44] C. Bu, D. Liu, X. Chen, D. Pallarès, A. Gómez-Barea, Ignition behavior of single coal particle in a fluidized bed under O_2/CO_2 and O_2/N_2 atmospheres: a combination of visual image and particle temperature, Appl. Energy 115 (2014) 301–308.
[45] M. Geier, C.R. Shaddix, K.A. Davis, H.-S. Shim, On the use of single-film models to describe the oxy-fuel combustion of pulverized coal char, Appl. Energy 93 (2012) 675–679.
[46] A. Molina, C.R. Shaddix, Ignition and devolatilization of pulverized bituminous coal particles during oxygen/carbon dioxide coal combustion, Proc. Combust. Inst. 31 (2007) 1905–1912.
[47] S. Bandyopadhyay, D. Bhaduri, Prediction of ignition temperature of a single coal particle, Combust. Flame 18 (1972) 411–415.
[48] C.R. Shaddix, A. Molina, Particle imaging of ignition and devolatilization of pulverized coal during oxy-fuel combustion, Proc. Combust. Inst. 32 (2009) 2091–2098.
[49] A. Ruscio, F. Kazanc, Y.A. Levendis, Comparison of fine ash emissions generated from biomass and coal combustion and valuation of predictive furnace deposition indices: a review, J. Energy Eng. 142 (2015) E4015007.
[50] M. Schiemann, N. Vorobiev, V. Scherer, Stereoscopic pyrometer for char combustion characterization, Appl. Opt. 54 (2015) 1097–1108.
[51] R. Khatami, Y.A. Levendis, An overview of coal rank influence on ignition and combustion phenomena at the particle level, Combust. Flame 164 (2016) 22–34.
[52] G. Wang, R. Zander, M. Costa, Oxy-fuel combustion characteristics of pulverized-coal in a drop tube furnace, Fuel 115 (2014) 452–460.
[53] F. Richter, G. Rein, Heterogeneous kinetics of timber charring at the microscale, J. Anal. Appl. Pyrolysis 138 (2019) 1–9.
[54] M. Dall'Ora, P.A. Jensen, A.D. Jensen, Suspension combustion of wood: influence of pyrolysis conditions on char yield, morphology, and reactivity, Energy Fuels 22 (2008) 2955–2962.
[55] R. Zanzi, K. Sjöström, E. Björnbom, Rapid high-temperature pyrolysis of biomass in a free-fall reactor, Fuel 75 (1996) 545–550.
[56] Y. Zhang, S. Kajitani, M. Ashizawa, K. Miura, Peculiarities of rapid pyrolysis of biomass covering medium-and high-temperature ranges, Energy Fuels 20 (2006) 2705–2712.
[57] A. Trubetskaya, P.A. Jensen, A.D. Jensen, A.D.G. Llamas, K. Umeki, P. Glarborg, Effect of fast pyrolysis conditions on biomass solid residues at high temperatures, Fuel Process. Technol. 143 (2016) 118–129.
[58] M.J. Wornat, R.H. Hurt, N.Y. Yang, T. Headley, Structural and compositional transformations of biomass chars during combustion, Combust. Flame 100 (1995) 131–143.
[59] R. Zanzi, K. Sjöström, E. Björnbom, Rapid pyrolysis of agricultural residues at high temperature, Biomass Bioenergy 23 (2002) 357–366.
[60] E. Cetin, B. Moghtaderi, R. Gupta, T. Wall, Influence of pyrolysis conditions on the structure and gasification reactivity of biomass chars, Fuel 83 (2004) 2139–2150.
[61] E. Cetin, R. Gupta, B. Moghtaderi, Effect of pyrolysis pressure and heating rate on radiata pine char structure and apparent gasification reactivity, Fuel 84 (2005) 1328–1334.
[62] E. Biagini, C. Fantozzi, L. Tognotti, Characterization of devolatilization of secondary fuels in different conditions, Combust. Sci. Technol. 176 (2004) 685–703.
[63] A.M. Janse, H.G. de Jonge, W. Prins, W.P. van Swaaij, Combustion kinetics of char obtained by flash pyrolysis of pine wood, Ind. Eng. Chem. Res. 37 (1998) 3909–3918.
[64] M. Guerrero, M. Ruiz, M. Alzueta, R. Bilbao, A. Millera, Pyrolysis of eucalyptus at different heating rates: studies of char characterization and oxidative reactivity, J. Anal. Appl. Pyrolysis 74 (2005) 307–314.
[65] E. Biagini, P. Narducci, L. Tognotti, Size and structural characterization of lignin-cellulosic fuels after the rapid devolatilization, Fuel 87 (2008) 177–186.
[66] E. Biagini, M. Simone, L. Tognotti, Characterization of high heating rate chars of biomass fuels, Proc. Combust. Inst. 32 (2009) 2043–2050.
[67] K. Umeki, K. Kirtania, L. Chen, S. Bhattacharya, Fuel particle conversion of pulverized biomass during pyrolysis in an entrained flow reactor, Ind. Eng. Chem. Res. 51 (2012) 13973–13979.
[68] K. Davidsson, J. Pettersson, Birch wood particle shrinkage during rapid pyrolysis, Fuel 81 (2002) 263–270.
[69] C. Mock, H. Lee, S. Choi, V. Manovic, Combustion behavior of relatively large pulverized biomass particles at rapid heating rates, Energy & Fuels 30 (12) (2016) 10809–10822.
[70] P. Mason, L. Darvell, J. Jones, M. Pourkashanian, A. Williams, Single particle flame-combustion studies on solid biomass fuels, Fuel 151 (2015) 21–30.
[71] P.E. Mason, L.I. Darvell, J.M. Jones, A. Williams, Observations on the release of gas-phase potassium during the combustion of single particles of biomass, Fuel 182 (2016) 110–117.
[72] D. Magalhães, A. Panahi, F. Kazanç, Y.A.J.F. Levendis, Comparison of single particle combustion behaviours of raw and torrefied biomass with turkish lignites, Fuel 241 (2019) 1085–1094.
[73] J. Riaza, R. Khatami, Y.A. Levendis, L. Álvarez, M.V. Gil, C. Pevida, F. Rubiera, J.J. Pis, Combustion of single biomass particles in air and in oxy-fuel conditions, Biomass Bioenergy 64 (2014) 162–174.
[74] F.F. Costa, M. Costa, Particle fragmentation of raw and torrefied biomass during combustion in a drop tube furnace, Fuel 159 (2015) 530–537.
[75] F.F. Costa, G. Wang, M. Costa, Combustion kinetics and particle fragmentation of raw and torrified pine shells and olive stones in a drop tube furnace, Proc. Combust. Inst. 35 (2015) 3591–3599.
[76] O. Karlström, M. Costa, A. Brink, M. Hupa, CO_2 gasification rates of char particles from torrefied pine shell, olive stones and straw, Fuel 158 (2015) 753–763.
[77] A. Carvalho, M. Rabaçal, M. Costa, M.U. Alzueta, M. Abián, Effects of potassium and calcium on the early stages of combustion of single biomass particles, Fuel 209 (2017) 787–794.
[78] T. Botelho, M. Costa, M. Wilk, A. Magdziarz, Evaluation of the combustion characteristics of raw and torrefied grape pomace in a thermogravimetric analyzer and in a drop tube furnace, Fuel 212 (2018) 95–100.
[79] N. Vorobiev, A. Becker, H. Kruggel-Emden, A. Panahi, Y.A. Levendis, M. Schiemann, Particle shape and stefan flow effects on the burning rate of torrefied biomass, Fuel 210 (2017) 107–120.
[80] G. Vizzini, A. Bardi, E. Biagini, M. Falcitelli, L. Tognotti, Prediction of rapid biomass devolatilization yields with an upgraded version of the bio-CPD model, Combustion Institute, 2008 Italian Section.
[81] C. Dupont, L. Chen, J. Cances, J.-M. Commandre, A. Cuoci, S. Pierucci, E. Ranzi, Biomass pyrolysis: kinetic modelling and experimental validation under high temperature and flash heating rate conditions, J. Anal. Appl. Pyrolysis 85 (2009) 260–267.
[82] E. Ranzi, M. Corbetta, F. Manenti, S. Pierucci, Kinetic modeling of the thermal degradation and combustion of biomass, Chem. Eng. Sci. 110 (2014) 2–12.
[83] P.T. Williams, A.R. Reed, High grade activated carbon matting derived from the chemical activation and pyrolysis of natural fibre textile waste, J. Anal. Appl. Pyrolysis 71 (2004) 971–986.
[84] P. Fu, S. Hu, J. Xinag, L. Sun, T. Yang, A. Zhang, Y. Wang, G. Chen, Effects of pyrolysis temperature on characteristics of porosity in biomass chars, International Conference on Energy and Environment Technology, ICEET'09, IEEE (2009), pp. 109–112.
[85] M. Momeni, C. Yin, S. Knudsen Kær, S.L. Hvid, Comprehensive study of ignition and combustion of single wooden particles, Energy Fuels 27 (2013) 1061–1072.
[86] M. Schiemann, S. Haarmann, N. Vorobiev, Char burning kinetics from imaging pyrometry: particle shape effects, Fuel 134 (2014) 53–62.
[87] Y.A. Levendis, R.C. Flagan, Synthesis, formation and characterization of micron-sized glassy carbon spheres of controlled pore structure, Carbon 27 (1989) 265–283.
[88] I. Smith, The combustion rates of coal chars: a review, Symp. (Int.) Combust. 19 (1982) 1045–1065.
[89] A. Panahi, Y.A. Levendis, N. Vorobiev, M. Schiemann, Direct observations on the combustion characteristics of miscanthus and beechwood biomass including fusion and spherodization, Fuel Process. Technol. 166 (2017) 41–49.
[90] A. Panahi, Y.A. Levendis, N. Vorobiev, M. Schiemann, V. Scherer, Combustion behaviors of a herbaceous and a woody biomass, in: B.A. Sakkestad (Ed.), 41st International Technical Conference on Clean Coal & Fuel Systems, Clearwater, Florida, USA (2016), pp. 62–72.
[91] N. Vorobiev, M. Geier, M. Schiemann, V. Scherer, Experimentation for char combustion kinetics measurements: bias from char preparation, Fuel Process. Technol. 151 (2016) 155–165.
[92] L.E. Arteaga-Pérez, C. Segura, V. Bustamante-García, O.G. Cápiro, R. Jiménez, Torrefaction of wood and bark from eucalyptus globulus and eucalyptus nitens: focus on volatile evolution vs feasible temperatures, Energy 93 (2015) 1731–1741.
[93] F. Kazanc, R. Khatami, P. Manoel Crnkovic, Y.A. Levendis, Emissions of NO_x and SO_2 from coals of various Ranks, Bagasse, and coal-bagasse blends burning in O_2/N_2 and O_2/CO_2 environments, Energy Fuels 25 (2011) 2850–2861.
[94] R. Khatami, C. Stivers, K. Joshi, Y.A. Levendis, A.F. Sarofim, Combustion behavior of single particles from three different coal ranks and from sugar cane bagasse in O_2/N_2 and O_2/CO_2 atmospheres, Combust. Flame 159 (2012) 1253–1271.
[95] Y.A. Levendis, K.R. Estrada, H.C. Hottel, Development of multicolor pyrometers to monitor the transient response of burning carbonaceous particles, Rev. Sci. Instrum. 63 (1992) 3608–3622.
[96] R. Khatami, Y.A. Levendis, M.A. Delichatsios, Soot loading, temperature and size of single coal particle envelope flames in conventional-and oxy-combustion conditions (O_2/N_2 and O_2/CO_2), Combust. Flame 162 (2015) 2508–2517.
[97] R. Khatami, Y.A. Levendis, On the deduction of single coal particle combustion temperature from three-color optical pyrometry, Combust. Flame 158 (2011) 1822–1836.
[98] B. Ma, M.B. Long, Absolute light calibration using S-type thermocouples, Proc. Combust. Inst. 34 (2013) 3531–3539.

[99] P.G.M. Database, Emissivity v temperature graph for platinum, (2016).
[100] Y.A. Levendis, K. Joshi, R. Khatami, A.F. Sarofim, Combustion behavior in air of single particles from three different coal ranks and from sugarcane bagasse, Combust. Flame 158 (2011) 452–465.
[101] D.L. Klass, Biomass for renewable energy, fuels, and chemicals, Elsevier, 1998.
[102] R.E. Mitchell, W.J. McLean, Temperature measurements of single pulverized–fuel particles by two-color pyrometry: II. Particle-burning behavior, Sandia National Labs., Livermore, CA, USA, 1983.
[103] R.E. Mitchell, Experimentally determined overall burning rates of coal chars, Combust. Sci. Technol. 53 (1987) 165–186.
[104] M.V. Gil, J. Riaza, L. Álvarez, C. Pevida, F. Rubiera, Biomass devolatilization at high temperature under N_2 and CO_2: char morphology and reactivity, Energy 91 (2015) 655–662.
[105] A.R. Reed, P.T. Williams, Thermal processing of biomass natural fibre wastes by pyrolysis, Int. J. Energy Res. 28 (2004) 131–145.
[106] J. Lédé, H.Z. Li, J. Villermaux, H. Martin, Fusion-like behaviour of wood pyrolysis, J. Anal. Appl. Pyrolysis 10 (1987) 291–308.
[107] R. Narayan, M.J. Antal, Thermal lag, fusion, and the compensation effect during biomass pyrolysis, Ind. Eng. Chem. Res. 35 (1996) 1711–1721.
[108] K. Maliutina, A. Tahmasebi, J. Yu, Effects of pressure on morphology and structure of bio-char from pressurized entrained-flow pyrolysis of microalgae, Data Brief 18 (2018) 422–431.
[109] P. McNamee, L. Darvell, J. Jones, A. Williams, The combustion characteristics of high-heating-rate chars from untreated and torrefied biomass fuels, Biomass Bioenergy 82 (2015) 63–72.
[110] T.U.S.P.C.U.-S.-N. 616, <616>Bulk density and tapped density of powders, (2014).
[111] A. Downie, A. Crosky, P. Munroe, Physical properties of biochar, Biochar for Environmental Management: Science and Technology, Earthscan, 2009, pp. 13–32. www.earthscan.co.uk.
[112] O. Senneca, B. Apicella, C. Russo, F. Cerciello, P. Salatino, S. Heuer, A. Wütscher, M. Schiemann, M. Muhler, V. Scherer, Pyrolysis and thermal annealing of coal and biomass in CO_2-rich atmospheres, Energy Fuels 32 (2018) 10701–10708.
[113] T.R. Ballantyne, P.J. Ashman, P.J. Mullinger, A new method for determining the conversion of low-ash coals using synthetic ash as a tracer, Fuel 84 (2005) 1980–1985.
[114] H. Kobayashi, J. Howard, A.F. Sarofim, Coal devolatilization at high temperatures, Symp. (Int.) Combust. 16 (1977) 411–425.
[115] A. Becker, M. Schiemann, V. Scherer, C. Shaddix, D. Haxter, J. Mayer, Comparative ignition tests of coal under oxy-fuel conditions in a standardized laboratory test rig, Fuel 208 (2017) 127–136.
[116] A. Zheng, Z. Zhao, Z. Huang, K. Zhao, G. Wei, X. Wang, F. He, H. Li, Catalytic fast pyrolysis of biomass pretreated by torrefaction with varying severity, Energy Fuels 28 (2014) 5804–5811.
[117] S.B. Liaw, H. Wu, A new method for direct determination of char yield during solid fuel pyrolysis in drop-tube furnace at high temperature and its comparison with ash tracer method, Energy Fuels 33 (2019) 1509–1517.
[118] Y. Liu, M. Geier, A. Molina, C.R. Shaddix, Pulverized coal stream ignition delay under conventional and oxy-fuel combustion conditions, Int. J. Greenh. Gas Control 5 (2011) S36–S46.
[119] R.H.J.C. Essenhigh, Influence of initial particle density on the reaction mode of porous carbon particles, Combust. Flame 99 (1994) 269–279.
[120] J.G. Pohlmann, E. Osório, A.C. Vilela, M.A. Diez, A.G. Borrego, Pulverized combustion under conventional (O2/N2) and oxy-fuel (O2/CO2) conditions of biomasses treated at different temperatures, 155 (2017) 174–182.
[121] O. Senneca, F. Cerciello, L. Cortese, S. Heuer, M. Schiemann, V. Scherer, Effects of CO_2 enriched atmosphere on chars from walnut shells pyrolysis in a drop tube reactor, Fuel 229 (2018) 235–240.
[122] J. Yu, J.A. Lucas, T.F. Wall, Formation of the structure of chars during devolatilization of pulverized coal and its thermoproperties: a review, Prog. Energy Combust. Sci. 33 (2007) 135–170.
[123] T.F. Wall, G.-S. Liu, H.-W. Wu, D.G. Roberts, K.E. Benfell, S. Gupta, J.A. Lucas, D.J. Harris, The effects of pressure on coal reactions during pulverised coal combustion and gasification, Prog. Energy Combust. Sci. 28 (2002) 405–433.
[124] M. Rabaçal, M. Costa, M. Vascellari, C. Hasse, M. Rieth, A.M. Kempf, A large eddy simulation study on the effect of devolatilization modelling and char combustion mode modelling on the structure of a large-scale, biomass and coal co-fired flame, J. Combust. 2018 (2018) 15, doi:10.1155/2018/7036425.
[125] G. Tufano, O. Stein, A. Kronenburg, G. Gentile, A. Stagni, A. Frassoldati, T. Faravelli, A. Kempf, M. Vascellari, C. Hasse, Fully-resolved simulations of coal particle combustion using a detailed multi-step approach for heterogeneous kinetics, Fuel 240 (2019) 75–83.
[126] T. Sayadi, S. Farazi, S. Kang, H. Pitsch, Transient multiple particle simulations of char particle combustion, Fuel 199 (2017) 289–298.
[127] M. Rieth, M. Rabacal, A. Kempf, A. Kronenburg, O. Stein, Carrier-phase DNS of biomass particle ignition and volatile burning in a turbulent mixing layer, Chem. Eng. Trans. 65 (2018) 37–42.
[128] L. Baxter, Biomass-coal co-combustion: opportunity for affordable renewable energy, Fuel 84 (2005) 1295–1302.